Slow Relaxation and Aging Phenomena at the Nanoscale in Granular Materials

V. Y. Zaitsev,[1,2,3,*] V. E. Gusev,[2] V. Tournat,[2] and P. Richard[4]
[1]Institute of Applied Physics, RAS, Uljanova St. 46, 603950 Nizhny Novgorod, Russia
[2]LUNAM Université, Université du Maine, CNRS, LAUM UMR 6613, avenue O. Messiaen, 72085 Le Mans, France
[3]Nizhny Novgorod State University, avenue Gagarina 23, 603950 Nizhny Novgorod, Russia
[4]LUNAM Université, IFSTTAR, site de Nantes, Route de Bouaye CS4, 44344 Bouguenais Cedex, France
(Received 29 March 2013; published 14 March 2014)

Granular matter exhibits a rich variety of dynamic behaviors, for which the role of thermal fluctuations is usually ignored. Here we show that thermal fluctuations can pronouncedly affect contacting nanoscale asperities at grain interfaces and brightly manifest themselves through the influence on nonlinear-acoustic effects. The proposed mechanism based on intrinsic bistability of nanoscale contacts comprises a wealth of slow-dynamics regimes including slow relaxations and aging as universal properties of a wide class of systems with metastable states.

DOI: 10.1103/PhysRevLett.112.108302 PACS numbers: 83.80.Fg, 43.25.+y, 45.70.-n, 83.10.Tv

Introduction.—Slow relaxation phenomena in granular systems are of considerable interest to understand the physics of complex glassy-type systems [1], for which they act as macroscopic analogs of ensembles of atoms and molecules [2]. Granular systems are also crucial in many industrial and geophysical applications. Particularly, sufficiently ample understanding of nonlinear dynamics of individual contacts is required to interpret such intriguing and poorly understood phenomena as triggering of earthquakes by elastic waves with amplitudes significantly smaller than the damage threshold for rocks [3,4]. Compared to the widely studied slow macroscopic (i.e., grain-scale) rearrangements causing compaction of granular materials [2,5–8], processes at nanoscale potentially driven by weak strains, including natural thermal fluctuations, are much less studied. The latter are reasonably believed irrelevant to grain rearrangements during compaction and jamming-unjamming transitions [2,9]. However, using appropriate acoustic techniques, spontaneous thermally activated nanoscale processes can also be macroscopically observed. In particular, observations of slow relaxation of the elastic modulus in laboratory samples with cemented granular structure [10] as well as similar effects in field measurements in sandy soil on a scale of ~10 m [11] are known. High-intensity acoustic "conditioning" [10] or a mechanical impact [11] ruptured the weakest bonds and produced perturbations in the elastic moduli of order 10^{-6}–10^{-3} that were rather problematic to monitor. To overcome this experimental difficulty, a parameter dominated by the weak-bond-network rather than the stable material skeleton is highly desirable.

Here, we report (i) implementation of such an unconventional experimental approach, (ii) a model of individual-contact bistability having essentially new features compared with conventional ones discussed for AFM tips and adhesion hysteresis, and (iii) results of numerical simulations of collective behavior of such bistable contacts. These results capture essential observed features, in particular, the abrupt breaking of the nanoscale contacts, their slow post-shock restoration and the peculiar aging of the system, and the damage accumulation produced by repeated weak perturbations.

Methods.—Experimentally, we use an acoustic (usually *P*-wave) component produced by the material's own nonlinearity, which is strongly dominated by the contributions of the weakest-contact fraction [12,13]. Thus, amplitude variations of the nonlinear component, characterize temporal variations in the amount of contributing weak contacts. Compared with intact homogeneous solids, nonlinearity of granular packings is giant and can be observed much easier. Feasibility of such nonlinear-acoustic sounding was demonstrated in Ref. [14] using the nonlinear cross-modulation technique to monitor structural perturbations in granular material bulk induced by weak mechanical shocks. Another, practically simpler, nonlinear-demodulation technique was successfully applied for studying fine structural changes— avalanche precursors— in slowly tilted granular packings [15,16].

Here, the sounding technique [15,16], combined with pulse-type perturbations [14], is used to study slow relaxation of the weak-bond network in granular material with particular attention to the aging of material undergoing repeated perturbations [16]. We use random packings of glass beads 1 and 2 mm in diameter placed in a container 5–10 l in volume, to which a small electromagnetic shaker is attached. It produces perturbing pulses that are much weaker compared to typical conditions of tap-induced compaction [2,5–7] and surely do not cause macroscopic grain rearrangements. The strain amplitude of the pulses varied in different measurements from about 10^{-7} to 10^{-6} and their duration is 20 ms. The primary amplitude-modulated wave is at strain amplitude $\tilde{\epsilon}_A \sim 10^{-8}$–$10^{-7}$

(see also Ref. [17]). Unlike observations of the primary wave [10,11] dominated by the medium skeleton, we use the demodulated component that is strongly dominated by the weakest contacts in the material. This is confirmed by the fact that such moderate shocks with nanometer and even subnanometer displacements, which are able to break only the weakest contacts, can cause several-times drops in the demodulated-component amplitude. Thus, such drops are proportional to the number of shock-ruptured weak contacts (see also Ref. [15]), and the slow relaxation of the nonlinear-component amplitude reflects how those contacts are restored.

Figure 1 shows examples of slow relaxation in granular materials, observed via the amplitude of their nonlinear-acoustic response. If time t is counted from the shock endings, the latter amplitude demonstrates power-law rates close to $1/t^{1+n}$ with $|n| \ll 1$, i.e., close to log-time behavior corresponding to $n = 0$. Plots (a) and (c) demonstrate peculiar weakening of the material reaction to series of identical taps, i.e., a kind of "aging." Besides, plots (a) and (b) show that the nonlinearity-produced signal is much more sensitive to the state of weakest contacts than the fundamental component variability. Concerning the gradual relaxation of the shock-induced perturbations, we note that even if the probing signal is switched off just after the shock and switched on after a pause, the nonlinearity of the material restores spontaneously. This shows that the influence of the probing wave does not dominate the effect, although high-intensity acoustic strains (say 10^{-5}) may perturb the weak bonds [10,17,18].

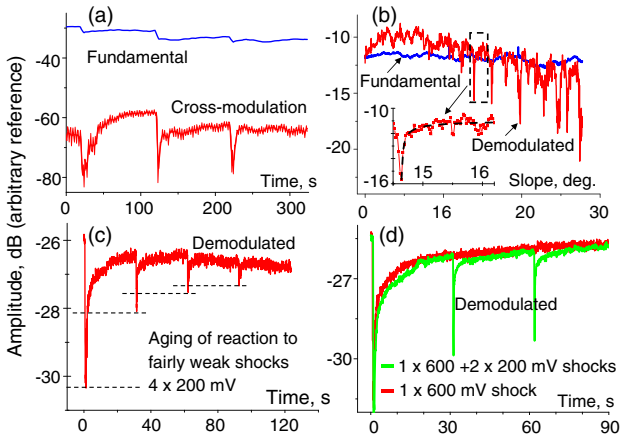

FIG. 1 (color online). Monitoring of slow relaxations via nonlinear-acoustic signal: (a) after perturbing shocks using cross-modulation technique [14]; (b) due to internal microslips in slowly tilted granular packings observed using demodulation technique [15,16]; (c) similarly observed "aging" of the system response to a series of identical fairly weak shocks, and (d) relaxation after one stronger shock and two weaker shocks that perturb barriers with essentially different energies. Notice much weaker perturbation of fundamental (linear) components shown in panels (a) and (b) for comparison.

Mechanism.—Under room temperature $T \sim 300$ K the characteristic thermal energy $k_B T$ (k_B being the Boltzmann constant) unambiguously indicates that thermal fluctuations cannot affect the state of visible, even weakly loaded, macroscopic contacts usually considered in granular matter modeling [9,19]. Thus only nanoscale surface asperities (from tens to hundreds of nanometers) can be considered as candidates of bistable structural elements potentially sensitive to thermal fluctuations. To understand the origin of their bistability, the analogy with the bistable behavior of tips in atomic-force microscopy (AFM) is very useful. For a tip already compressed by the contacting solid, the Hertzian force is repulsive, whereas the tip yet approaching a solid surface experiences the influence of short-range attraction forces. This attraction force for an AFM tip approaching another solid is equilibrated by the elasticity of the cantilever [dashed lines in Fig. 2(a)]. If the cantilever is soft enough, a bistability zone for the initial position $A_1 \le A \le A_2$ of the unstressed cantilever can appear [20] as illustrated in Fig. 2(a). In this zone, the cantilever can equilibrate the attraction force at two positions of the tip, "closed" and "open." Note that, in the latter position, the attraction force is almost absent. If the cantilever is moved forth and back, peculiar hysteretic jumps between the two positions occur [arrows in Fig. 2(a)]. Inside the bistability

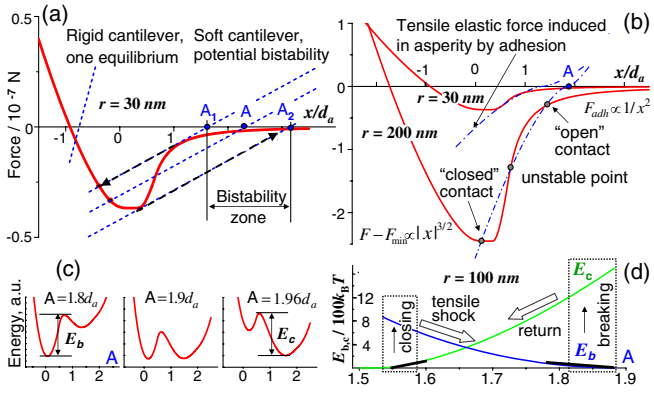

FIG. 2 (color online). Schematic elucidation of the contact-bistability origin. (a) Adhesion or compression force (solid line) for a small asperity ($r = 30$ nm) and equilibrating elastic force of a cantilever (dashed lines) which jointly are able to produce bistable equilibria if the cantilever is soft enough (the most-right and most-left intersection points). The elastic parameters and surface energy used are those of glass. (b) Elucidation that Hertzian-like elastic *tensile* force for sufficiently large contacts subjected to short-range adhesion forces from an opposite solid surface can also form bistable equilibria. (c) Corresponding two-minimum potential wells, for which the energy barriers $E_{b,c}$ exhibit opposite trends as a function of separation A normalized to atomic size d_a. (d) Energy barriers $E_b(A)$ and $E_c(A)$ that should be overcome to break "closed" contacts and close "open" ones. Dashed rectangles show low-energy regions in which thermal fluctuations can induce jumps to the opposite equilibrium.

zone sufficiently strong thermal fluctuations can cause transitions between the two equilibrium states.

At first glance, for nanoscale asperities at grain surfaces, there is no "soft cantilever" to create bistable equilibria like in AFM. However, as argued in Ref. [21], the elastic energy stored in compressed contacts scales like $h^{5/2}$, h being the displacement of the contact apex. Accordingly, the elastic force F_{comp} follows the Hertzian law $F_{\mathrm{comp}} \propto h^{3/2}$. But the same arguments applied to a contact apex displaced by the value $|h| = |x - A|$ due to a localized attractive force also lead to the appearance of an elastic force $F_{\mathrm{tens}} \propto |x - A|^{3/2}$ that equilibrates the attraction [dash-dotted curves in Fig. 2(b)]. Unlike AFM cantilever elasticity, this elastic force is nonlinear; i.e., initially it can be sufficiently soft to create the second (distant) equilibrium position for the contact tip. For AFM tips with the typical radius $r \lesssim 10$ nm, however, this "nonlinear spring" hidden inside the tip is insufficiently soft relative to adhesion, so that only an in-sequence connected soft cantilever can create the second potential minimum. But for a larger contact radius $r \gtrsim 30$–50 nm, due to a different dependence on r for the attraction and the "hidden spring," the latter becomes sufficiently soft relative to the adhesion force [compare the curves for $r = 30$ nm and $r = 200$ nm in Fig. 2(b)]. Thus, for the larger contacts, bistable equilibria can appear in a finite range of separations between the asperity apex and the opposite surface without the necessity of an artificial soft spring or cantilever. Figure 2(c) schematically shows how the resulting two-minima potential evolves with the initial separation A. These representations suggest a physically clear interpretation of the well-known [22] transition from the so-called Derjaguin-Muller-Toporov (DMT) model of very small contacts not having bistability to the Johnson-Kendall-Roberts (JKR) model for larger contacts exhibiting adhesion hysteresis [22]. The latter can be viewed as a special case of mechanical hysteresis, like for AFM tips, but arising without an artificial soft cantilever.

For elastic and surface energy typical of glasslike materials, contacts with $r \sim 10^2$ nm and $T \sim 300$ K exhibit narrow regions near the boundaries of the bistability zone, where one of the potential wells [E_b or E_c, see Fig. 2(b)] is 10^2 to 10^4 times larger than k_BT, while the other is of order $10^1 k_BT$. Thus, near the left boundary of the bistability region the closed state is much stabler, whereas the open one is metastable. Near the right boundary, the situation is the opposite. The metastable equilibrium energy is comparable with that of thermal fluctuations. So, they are able to induce jumps to the opposite stabler state with characteristic waiting times $\tau_0 \exp(E_{b,c}/k_BT)$ according to the Arrhenius law, where the attempt time for nanometer-scale tips of the asperities can reasonably be $\tau_0 \sim 10^{-12}$s.

Direct AFM inspection of the glass-bead surfaces confirmed the presence of numerous asperities about 10^2 nm in radius and 20–50 nm in height (see Ref. [23]) consistent with the values reported in Ref. [24]. A single macrocontact between two grains leads to 10^3–10^4 microasperities. Even if 1% of them actually get in contact, one obtains $\sim 10^2$ of such nanoscale contacts for a visible one. Following Refs. [13,15] we conclude that contribution of such loose but numerous nanocontacts can dominate over the nonlinearity of much stronger (and thus less nonlinear) macrocontacts creating the material skeleton. This explains why nonlinearity can drop drastically after fairly weak shocks that still leave the material skeleton intact, but suffice to break the nanocontacts.

Contour arrows in Fig. 2(d) schematically show the physical meaning of the relaxational closing of open contacts and the destructive action of perturbing weak tensile shocks, which do not completely get the system out of the bistability region. We recall that even for large nanocontacts (with $r \gtrsim 10^2$ nm), the bistality zone is of order of atomic size. Note that for characteristic attempt times $\tau_0 \sim 10^{-12}$ s and waiting times below tens of hours, only "active" contacts with barriers $\lesssim 45 k_BT$ can participate in thermally induced transitions. Then the narrow "active" parts of the energy curves near the bistability-region boundaries can be fairly well approximated by straight segments [thick solid lines in Fig. 2(d)]. Consequently, in such narrow regions for almost arbitrary distributions of the asperities' heights, the density of energy states for the active nanocontacts can be approximated as constant.

Kinetic Monte Carlo approach.—Using a kinetic Monte Carlo approach, we simulated transitions between "open" or "closed" states [see Figs. 2(b) and 2(d)] for 3×10^4 contacts. The probabilities of interstate jumps are given by the aforementioned Arrhenius law. If initially all nanoscale contacts are broken, the broken-contact density $N_b(E) = 1$ and population of closed contacts is zero, $N_c(E) = 0$. Gradual closing of the broken contacts starts from smallest energy barriers and looks like the motion of the steplike curve $N_b(E)$—"closing front"—towards the right boundary of the bistability zone with larger barriers. As argued above, the nonlinear-signal amplitude is proportional to the number of closed nanocontacts $\int N_c(E)dE$. Curves 1 in Figs. 3(b) and 3(d) show the closing front positions after 30 s and 1500 s of the initial relaxation, respectively. For contacts corresponding to the current position of the relaxation front that moves from the left boundary of the bistability zone to the right [Figs. 3(c) and 3(d), curves 1], the energy wells are deep for the open states and shallow for closed ones [see Fig. 2(d), left side]. Sufficiently strong tensile perturbations temporarily shift the nanocontacts towards the right boundary of the energy diagram where, in contrast, energy wells for closed states are shallow [Fig. 2(d), right side]. Consequently, transitions of previously closed contacts back to open states are fostered. As a result, at the end of a shock, the preshock position of the closing front [Figs. 3(b) and 3(d), curves 1] is shifted back to the left [Figs. 3(b) and 3(d), curves 2], but then the

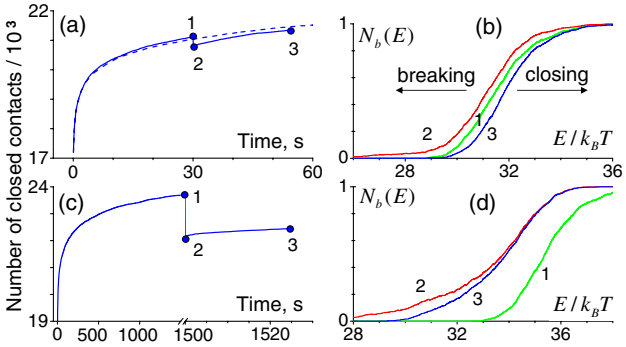

FIG. 3 (color online). Evolution of the number of closed nanoscale contacts (left) and populations $N_b(E)$ of broken ones (right). Upper and lower rows are for the just prepared packing with $N_b(E) = 1$ relaxed during 30 s and 1500 s, respectively. In both cases the same fairly weak perturbing shock that breaks only a portion of earlier closed contacts is applied. Labels 1 and 2 are for the system state just before and just after the shock. Labels 3 are for the system states 24 s after the shock. Compare experimental Fig. 1(d) with Fig. 3(a), where the dashed curve shows continuous relaxation. Note the much smaller difference between states 2 and 1 for the initial relaxation time 30 s [(a) and (b)] than for 1500 s [(c) and (d)].

closing front continues its movement to the right. For the same shock duration and amplitude, the resulting amount of the broken contacts that increases $N_b(E)$ essentially depends on the position of the closing front just before the shock (compare the upper and lower rows in Fig. 3).

Even stronger perturbations can already shift all bistable contacts to the right beyond the bistability zone and break all earlier closed contacts. Since the width of the bistability zone is of the order of an atomic size, such strong shocks correspond to strains $\gtrsim 10^{-6}$–10^{-5} for millimetric grains. For weaker shocks, the system response can be rather multivariant depending on shock amplitude, duration, and previous history. For example, besides the difference in the amounts of broken contacts, Fig. 3(b) shows that, by the same post-shock relaxation time, the closing front (curve 3) gets already to the right from its initial position [curve 1 in Fig. 3(b)] in contrast to the opposite situation in Fig. 3(d). Next, let us recall that besides the difference in the barrier energies $E_{b,c}$ the widths of bistability zones can strongly differ for different contact sizes. Depending on that width, the same perturbation can be "strong" or "weak," so that perturbation or relaxation regimes for such fractions of bistable elements are quite different.

For the discussed features, the "aging" of the relaxation response to repeated weak shocks breaking small contact portions is a natural consequence. Such multiple weak shocks applied to previously well-relaxed material [like in Figs. 3(c) and 3(d)] gradually shift the system state towards the one shown in Figs. 3(a) and 3(b). However, that state, for which the relaxed front 3 gets to the right from the initial position 1, is not reached and the system response saturates when the relaxation between the shocks becomes able to

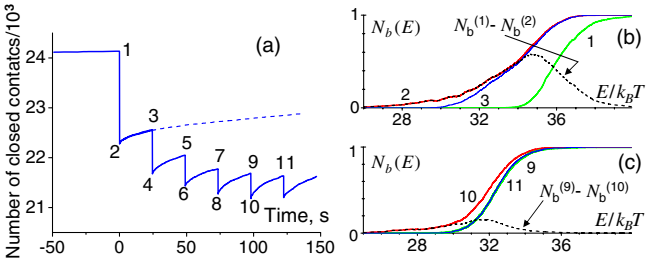

FIG. 4 (color online). Simulated "aging" of reaction to multiple weak shocks with accumulation of broken contacts for a well-relaxed (during 3×10^3 s) system. (a) is the time-domain representation similar to the experimental Fig. 1(c); (b) and (c) are the energy spectra of broken contacts. The mutually corresponding moments in plots (a), (b), and (c) are marked by the same numbers. Dashed lines in plots (b) and (c) show that the initial perturbation $N_b^{(1)}(E) - N_b^{(2)}(E)$ strongly exceeds $N_b^{(9)}(E) - N_b^{(10)}(E)$ in the "aged" state, and the "aged" relaxed spectra $N_b^{(9)}(E)$ and $N_b^{(11)}(E)$ nearly coincide.

heal the perturbation ΔN_b produced by every previous shock. This saturated value ΔN_b is significantly smaller than the initial reaction of the well-relaxed system to the first perturbing impact. The transition to such "aged" reaction of the system is shown in Fig. 4 for the simplest situation of identical nanoscale contacts for which the barriers differ only by initial separation A. This model fairly well reproduces the observed gradual "aging" of the system response to repeated weak shocks [see Fig. 1(c)].

Discussion and conclusions.—Even without externally applied shocks, the discussed mechanism of nanocontact destruction or restoration manifests itself in slowly tilted granular packings [15,16], where the avalanche precursors act as internal "shocks" followed by relaxations [see inset in Fig. 1(b)]. For periodical forth-and-back tilting below the critical angle, the demodulated-signal variations strongly decrease (become "aged"). However, after ~1 hour rest, during which the broken nanocontacts restore, the signal variations also significantly restore [16].

Above we focused on fairly weak perturbations, after which the contacts relax independently of each other. If a stronger shock breaks a significant portion of nanocontacts, the surfaces of macroscopic intergranular contacts can experience separation even greater than individual bistability-zone widths. Then the interstate jumps of nanocontacts are not independent, and really collective hysteretic or relaxational mechanisms become important as will be discussed elsewhere. But even for weak perturbations, the revealed mechanism demonstrates a rich variety of regimes, including the aging [1] that has a rather general nature. The considered bistability of nanoscale contacts is a universal feature of both nonconsolidated (sand-like) and cemented (sandstone-like) granular materials, as well as solids with cracks having contacts at their interfaces. This explains universality of slow-dynamics effects observed in those materials [3,10,11,14–16,25]. Understanding of the gradual accumulation of broken contacts due to multiple

weak perturbations, like in Fig. 4(a), opens prospects for the physical interpretation of such intriguing phenomena as dynamic earthquake triggering that is phenomenologically discussed in Ref. [3] and the influence of fairly weak seismo-acoustic stimulation on oil recovery from nearly depleted wells [26].

Support of ANR Grant No. 2010-BLAN-0927-01 and Grant No 11.G34.31.0066 of the Russian Federation Government is acknowledged. V. Z. acknowledges the invited-professor grant from the University Rennes-1. We thank J.-F. Bardeau for the help with AFM imaging.

*vyuzai@hydro.appl.sci-nnov.ru

[1] A. Amir, S. Borini, Y. Oreg, and Y. Imry, Phys. Rev. Lett. **107**, 186407 (2011); A. Amir, Y. Oreg, and Y. Imry, Proc. Natl. Acad. Sci. U.S.A. **109**, 1850 (2012).
[2] P. Richard, M. Nicodemi, R. Delannay, P. Ribière, and D. Bideau, Nat. Mater. **4**, 121 (2005).
[3] P. Johnson, X. Jia, Nature (London) **437**, 871 (2005).
[4] P. Johnson, H. Savage, M. Knuth, J. Gomberg, and C. Marone, Nature (London) **451**, 57 (2008).
[5] J. B. Knight, C. G. Fandrich, C. N. Lau, H. M. Jaeger, and S. R. Nagel, Phys. Rev. E **51**, 3957 (1995).
[6] P. Richard, P. Philippe, F. Barbe, S. Bourlès, X. Thibault, and D. Bideau, Phys. Rev. E **68**, 020301 (2003).
[7] P. Ribière, P. Richard, R. Delannay, D. Bideau, M. Toiya, and W. Losert, Phys. Rev. Lett. **95**, 268001 (2005).
[8] C. Inserra, V. Tournat, and V. Gusev, Appl. Phys. Lett. **92**, 191916 (2008).
[9] S. Deboeuf, O. Dauchot, L. Staron, A. Mangeney, and J.-P. Vilotte, Phys. Rev. E **72**, 051305 (2005).
[10] J. A. TenCate, E. Smith, and R. A. Guyer, Phys. Rev. Lett. **85**, 1020 (2000).
[11] V. S. Averbakh, A. V. Lebedev, A. P. Maryshev, and V. I. Talanov, Acoust. Phys. **55**, 211 (2009).
[12] V. Zaitsev, Acoust. Phys. **41**, 385 (1995).
[13] V. Tournat, V. Zaitsev, V. Gusev, V. Nazarov, P. Béquin, and B. Castagnède, Phys. Rev. Lett. **92**, 085502 (2004).
[14] V. Y. Zaitsev, V. E. Nazarov, V. Tournat, V. E. Gusev, and B. Castagnede, Europhys. Lett. **70**, 607 (2005).
[15] V. Y. Zaitsev, P. Richard, R. Delannay, V. Tournat, and V. E. Gusev, Europhys. Lett. **83**, 64003 (2008).
[16] S. Kiesgen de Richter, V. Yu. Zaitsev, P. Richard, R. Delannay, G. Le Caër, and V. Tournat, J. Stat. Mech. (2010) P11023.
[17] See Supplemental Material at http://link.aps.org/supplemental/10.1103/PhysRevLett.112.108302 for Supplemental file No 1 which contains discussion of experimental details for the nonlinear-sounding techniques used for obtaining the examples shown in Fig. 1.
[18] V. Tournat, V. E. Gusev, Phys. Rev. E **80**, 011306 (2009).
[19] L. Staron, J.-P. Vilotte, and F. Radjai, Phys. Rev. Lett. **89**, 204302 (2002).
[20] N. A. Burnham and A. J. Kulik, in *Surface Forces and Adhesion*, edited by B. Bhushan, Handbook of Micro/Nanotribology (CRC Press, Boca Raton, FL, 1999), ed. 2, pp. 247-71.
[21] K. L. Johnson, *Contact Mechanics* (Cambridge University Press, Cambridge, England, 1987).
[22] B. Deryagin, N. Churaev, V. Muller, and J. Kitchener, *Surface Forces* (Consultants Bureau, New York, 1987).
[23] See Supplemental Material at http://link.aps.org/supplemental/10.1103/PhysRevLett.112.108302 for Supplemental file No 2 which presents an AFM image showing that beads' surfaces have many submicrometer asperities with parameters consistent with the expected ones.
[24] T. Divoux, H. Gayvallet, and J.-C. Géminard, Phys. Rev. Lett. **101**, 148303 (2008).
[25] R. A. Guyer and P. A. Johnson, *Nonlinear Mesoscopic Elasticity. The Complex Behaviour of Rocks, Soil, Concrete* (Wiley-VCH, Weinheim, 2009).
[26] I. A. Beresnev and P. A. Johnson, Geophysics **59**, 1000 (1994).

Supplemental material - 1: Experimental setups and methods

Experimental methods used in the reported study are generically close those discussed in refs. [14-17] cited in the Letter, as well as in refs. [S1-S4] from the additional reference list given below. Those studies were aimed first of all on general understanding how intrinsic nonlinearity of granular materials generates nonlinear acoustic components. The latter have proven to be a very sensitive tool for studying fine modifications in the material inner structure, even if such modifications are not accompanied by any macroscopic grain rearrangements that were the focus of quite a number of studies in granular-material physics related to compaction and tamping of granular packings (see e.g. review [2]).

An attractive feature of the nonlinear-acoustic approach is that it opens a possibility to descend to much smaller scales of structural modifications. In contrast to linear approaches (e.g. acoustic microscopy or conventional pulse-echo ultrasonic methods used in nondestructive testing), in which the scales of the probed structural features are compared with the wavelength of the probing wave (or even the envelope of a pulse containing several periods), the nonlinear-acoustic approach suggests a much smaller scale. Namely, the role of the reference scale plays the displacement amplitude in the probing wave. For waves with lengths on the order of 10^{-2} m and strain amplitudes $\sim 10^{-7}$ (the latter being quite sufficient for observing nonlinear effects), the displacements have nanometer scale. This approach is especially useful if the studied material contains thin discontinuities like contacting surfaces at intergrain contacts or interfaces in cracks. Although the spatial resolution like in conventional linear sounding is still determined by the macroscopic wavelength, nonlinear-acoustic components can be strongly sensitive even to nano- and sub-nanometer displacements comparable with the particle-oscillation amplitude at the above-mentioned interfaces. This is the basis idea of studying nano-scale displacements at intergrain contacts using their macroscopic nonlinear-acoustic manifestations.

In principle, in granular materials one has a rather wide choice of nonlinear effects that can be used in observations. The list of such nonlinear effects comprises higher harmonic generation [S3-S5,13] (the most well-know effect), demodulation phenomena in CW and pulsed regimes [S1,S2,S4,14], cross-modulation effects [S6,15], amplitude and phase self-action [S7], etc. In particular, the simple effect of demodulation of an initially 100% amplitude-modulated carrier wave suggests a rather convenient possibility. Just this variant based on the observation of the amplitude of the demodulated (down-converted in frequency domain) component was used in the most part of the examples presented in Fig. 1 in the body text of the present Letter.

Figure S1 schematically shows the experimental setup that was mostly used in the reported studies in several slightly different modifications. The typical sizes of the container **1** were 30x20x20 cm. In the middle of the longer wall, two round holes were made in which two cylinder-shape piezo-transducers (Panametrics V3052 with an active surface radius a =1.75 cm) were tightly inserted. Transducer **2** served for radiation and transducer **4** for reception. An electromagnetic shaker **5** (B&K 4810) was attached to the container to produce perturbing pulses, mostly with a fixed duration of 20 ms. The latter value was smaller than the time step (typically 30-60 ms) between subsequently obtained Fourier spectra of the received signal. Usually the Stanford Research Systems signal analyzer SR785 was used for this purpose. The perturbing-pulse amplitude varied an order of magnitude in different experiments. Using the terminology of the Letter, the “fairly weak” perturbations obviously corresponded to the regime of smaller-voltage output of the generator of perturbing pulses (50-150 mV at the input of the amplifier controlling the shaker). In this regime, the average-compressed contacts composing the material skeleton still remained intact and only a small portion of the weakest bonds were broken. However, the nonlinear component could already drop within a few dB, whereas the variations of the fundamental component usually were barely noticeable. In this regime, the material response was especially well reproducible. For the largest perturbation amplitudes (500-700 mV at the input), the material response was less

reproducible and the magnitude of the observed variations was much larger (tens of dB for the nonlinear component and several dB for the linear component). The strain of both the probing waves and the perturbed pulses was estimated using a small accelerometer (B&K 4375) embedded at a depth of several centimeters from the packing surface. For estimates of the probing-wave amplitude, the accelerometer axis was oriented horizontally along the wave-beam propagation. For the perturbing shocks, the accelerometer axis was vertical along the impact direction. The estimated strain of weaker perturbing pulses 10^{-7}-10^{-6} remained at least 1-2 orders of magnitude smaller that the average static strain of intergrain contacts in the middle part of the container (at depths about 5-15 cm and larger).

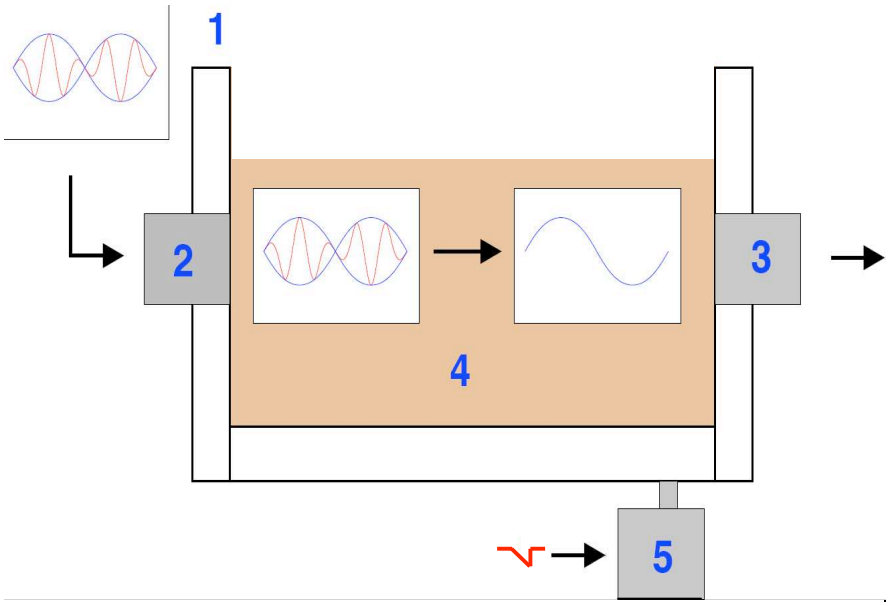

Fig. S1. Schematically shown experimental setup used in the observations of slow relaxation after perturbations produced by weak mechanical shocks. (1) is the container made of rigid plastic; (2) and (3) are the piezo-transducers used for radiation of the primary probing wave and reception of the nonlinear acoustic component generated in the material bulk due to nonlinearity of the granular matter (4) filling the container. Schematically shown are the input signal fed to the piezo-actuator (2) and the perturbing pulse fed to a small electromagnetic shaker (5) attached to the container.

For the 100% AM-modulated probing signal, the central-component frequency usually fell into the range 8-10 kHz, whereas the modulation frequency was 1-2 kHz. It should be emphasized that the transducer resonances were much higher, and the demodulation process is not highly frequency sensitive. Therefore, the exact choice of the frequencies was not critical and the main features of the observed phenomena were very well reproducible for different experiments. The propagation of acoustic waves in the low kHz range is definitely strongly dominated by the inter-granular contact network and not by the air filling the pores [18]. The analyzer SR785 ensured the possibility to memorize the sequences of up to 1944 spectra in the "waterfall" regime and compare the time dependences for the chosen spectral components by making temporal slices of the entire waterfall. Just such slices are presented in Fig. 1 in the Letter. This allowed us to easily study the processes within characteristic observation time $[t_{min}, t_{max}]$ ranged over 10^3 times. In linear measurements (like described in [11,12]) in order to obtain the acceptable observation accuracy, individual experimental points often can require signal averaging during at least several seconds or even more. Under such conditions even several hours of continuous measurements usually also ensure the relative time range 10^2-10^3 times comparable with our experiments.

In the discussed measurements, the granular material (4) consisting of glass beads was usually poured into the container and was not subjected to special procedures of tampimg/compaction. The time before

application of perturbing shocks and starting the measurements could vary from several minutes to several hours in different experiments. Qualitatively the material reaction to perturbations was similar for those cases. However, it was noticed that if for a freshly-prepared packing, the sounding signal was first switched on for a few seconds only and then switched on again after several hours of complete rest, the level of the nonlinear component could spontaneously increase rather significantly, up to 2-3 times and more. In other control experiments another type, the probing wave was switched for a few seconds with intermediate pauses of 20-60 seconds. It was verified that for such shorter observation periods (under the same other parameters), the non-linear signal level remained fairly stable within fractions of one dB. Even if a moderate (in the above-defined sense) perturbing shock was applied between those control measurements, the difference in the nonlinear-component level also remained comparable, and we never observed such strong drops of the nonlinear component as shown in examples in Fig. 1 just after the shock applied during continuous monitoring of the signal amplitude.

Such control experiments clearly indicate that the material relaxation was not noticeably affected by the influence of the sounding wave itself if the wave strain amplitude was sufficiently small (on the order 10^{-8}-10^{-7}), so that the relaxation process was mostly really spontaneous. However, in agreement with observations [18] we also noted that for sounding-wave amplitude closer to maximum available level with strains on the order of 10^{-6}, the sounding wave was already able to noticeably affect the relaxation and cause irregular variations in the nonlinear-component level as shown in Fig. S2.

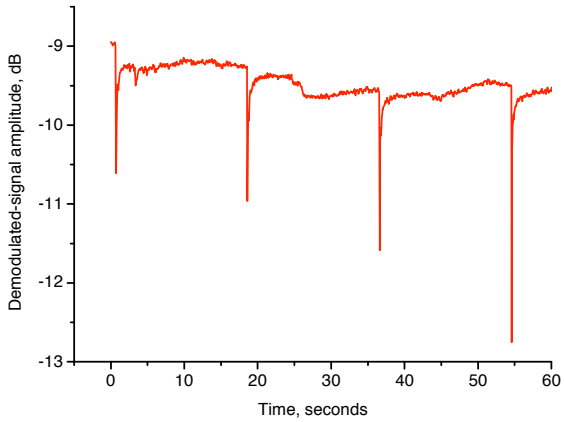

Fig. S2. A example of the demodulated-component behavior for the conditions similar to the examples in Fig. 1 in the Letter (i.e. applying perturbing shocks of similar ampllitude), but obtained using the maximum level of the sounding wave (with strain ~10^{-6}). For such elevated amplitudes, the probing wave itself already affected the state of the weak bonds and produced pronounced irregular variations in the amplitude of the demodulated component dominated by contributions of the weakest contacts.

Concerning the robustness of the observed effects, we note that usually compressional (P-type) probing wave was radiated, although it was verified that shear primary wave (S-type) can also be successfully used. In the latter case, for approximately isotropic materials, the symmetry conditions strongly suppress the even-order (first of all, quadratic) nonlinearity responsible for the generation of shear-type demodulated waves as well as the second harmonic. However, in such a case the nonlinear transformation into even harmonics or into demodulated components occurs with simultaneous conversion of the primary S-wave into compressional mode (see [14,S3]). For weakly-nonlinear consolidated solids, this effect is weak, but in highly-nonlinear granular materials such transformations are quite efficient even despite the mismatch between the velocities of compressional and shear modes.

In the context of universality of the material response to different types of perturbations, the example presented in Fig. 1b is obtained for strongly different type of perturbations. In this case, the granular packing was slowly inclined towards the critical angle (about 28-30 degrees) of the avalanche instability. The corresponding experiment configuration is shown in Fig. S3 (corresponding to the experiments described in refs. [16,17]).

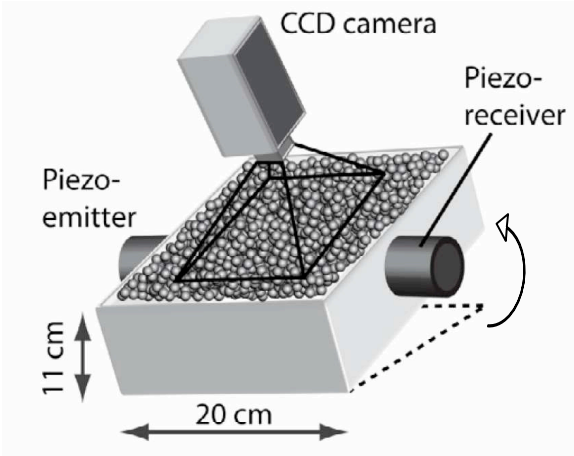

Fig. S3. Schematics of the experimental setup and formation of demodulated (difference-frequency) signal in the granular-material bulk for a biharmonic primary wave.

For the slowly inclined packing, tangential component of the elastic force gradually increased and exceeded the dry-friction limit for certain portions of weakest contacts in the material bulk. As a result, such contacts experience collective micro-slips as simulated in refs. [S8,S9] using a molecular-dynamic approach. Such micro-slips are initially very weak and do not produce macroscopic grain rearrangement in the bulk (although on the surface, quite well visible gradually increasing portions of grain may be displaced even fairly far from the critical angle of avalanche triggerning). However, microscopic perturbations of the weakest bonds produced by such events in the material bulk very pronouncedly affect generation of the nonlinear signal. The effect of those naturally arising "shocks" is very similar to that produced by artificially applied mechanical pulses. Each of such perturbations is followed by rapid drops in the material nonlinear-acoustic response, the level of which gradually restores much like after artificial shocks as shown in Fig. 1 in the Letter.

Concerning universality of the manifestation of breaking the weakest contacts for different nonlinear effects, Fig. 1a in the Letter demonstrates that very similar signal drops followed by slow restorations are also observed for the essentially different effect of cross-modulation [15, S6] (see also Fig. S4).

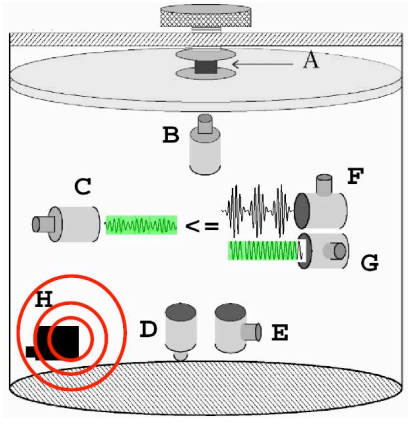

Fig. S4. Schematics of the experiment based on the cross-modulation effect consisting in the transfer of amplitude modulation from one carrier wave ("pump") to another initially non-modulated (probing) wave. We monitored the amplitude of the pump-induced modulation sidelobes of the probing wave. The perturbation-producing small shaker (H) and longitudinal piezo-transducers are similar to those used in the setup shown in Fig. S1. The shaker and the transducers were embedded in the granular material bulk (2 mm glass beads similar to the other experiments). The container was about 40 cm in diameter and height. Similar effects were observed for both co-propagating and orthogonally propagating waves. The distances between the radiating and receiving transducers were about 20 cm. The frequencies of the carrier waves were about 7 kHz and 10 kHz. Their roles can be interchanged since the interaction is not resonant. The modulation frequency was 30-40 Hz and the pump-induced sidelobes were observed using the waterfall regime of spectrum analyzer SR785 much like described above.

Additionally, in those experiments the packing was covered by a rigid lid which allowed for applying an external compressing force. The example presented in Fig.1a corresponds to the additional pressure about 10 kPa which is equivalent to the presence of an additional overburden material layer with thickness of about 0.6 m (i.e., an order of magnitude greater than for the free-laying material in the setup

shown in Figs. S1 and S3). However, even for such fairly strongly jammed material, the perturbing pulses of approximately the same intensity as mentioned above also caused well visible signal perturbations and subsequent relaxations that were definitely unrelated to the destruction of the material skeleton that was much stronger pre-strained.

Therefore, the ensemble of performed observations based on different acoustic effects and different ways for producing perturbations indicate that the revealed slow dynamics effects are rather reproducible and do not require any very special conditions or preparation protocols. Similar effects should manifest themselves in field conditions. The latter statement is confirmed by recent experiments [12] on a scale ~10 m, as well as by unpublished data obtained during earlier performed experiments [S7] for seismoacoustic waves (230 Hz) propagating in sandy soils along significantly longer paths up to 120-165 m. In those experiments, besides the "fast" amplitude-dependent effects reported in [S10] quite pronounced aftereffect was observed if the amplitude of the sounding wave was reduced from maximum to minimum level during observation cycles lasting 15-30 min. The maximum level corresponded to about 300 Wt radiated power of a monopole source located in a lake. Its acoutic radiation transformed from water into seismo-acoustic wave and propagated through the soil. The softening of the material observed via changes in the phase velocity for higher wave amplitudes did not disappear completely after reduction of the amplitude by 30-35dB from the maximum, so that some residual softening (similarly to laboratory data [11]) was clearly observed during at least several minutes, although the detailed times-dependences for the aftereffect was not studied.

Discussions and examples how the amplitudes of nonlinearity-induced acoustic-wave components relate to parameters of intergrain contacts, such as their static prestraining, oscillation regimes (without clapping or in clapping regime) can be found in refs. [S1-S3,S5] and are also touched in refs. [13,14,16] cited in the Letter. However, for the present consideration, it is sufficient to take into account that in real granular packings containing differently loaded contacts, the linear elastic moduli are mostly determined by the visible average-loaded intergrain contacts that form the granular-material skeleton. In contrast, the weakest, least-loaded contacts give much smaller contribution to the linear elastic moduli, but their contribution can strongly dominate the material nonlinearity and thus the amplitude of nonlinearity-induced signal components [13-16, S1-S4]. Simple estimates presented in Supplemental file-2 confirm that for the discussed experimental conditions, the contribution of the weak contacts formed by nano-scale asperities of the glass-bead surfaces strongly dominates the amplitude of the observed nonlinearity-induced signal component. Consequently, in the section devoted to the kinetic Monte-Carlo simulations, one can consider that the variations in the number of closed nano-contacts are directly proportional to variations in the amplitude of the experimentally observed nonlinear signal components shown in Fig. 1.

S1. V. Y. Zaitsev, Nazarov V.E., and A. B. Kolpakov, "Detection of acoustic pulses in river sand: Experiment," Acoust. Phys. **45**, 235–241 (1999).

S2. V. Y. Zaitsev, A. B. Kolpakov, and V. E. Nazarov, "Detection of acoustic pulses in river sand. Theory," Acoust. Phys. **45**, 305–310 (1999).

S3. V. Tournat, V. E. Gusev, V. Y. Zaitsev, and B. Castagnède, "Acoustic second-harmonic generation with shear to longitudinal mode conversion in granular media," Europhysics Letters (EPL) **66**, 798–804 (2004).

S4. V. Tournat, V. Y. Zaitsev, V. E. Nazarov, V. E. Gusev, and B. Castagnéde, "Experimental Study of Nonlinear Acoustic Effects in a Granular Medium," Acoustical Physics **51**, 543 (2005).

S5. I. Y. Belyaeva, V. Y. Zaitsev, and E. M. Timanin, "Experimental Study of Nonlinear Elastic Properties of Grainy media with Nonideal Packing," Acoust. Phys. **40**, 789–793 (1994).

S6. V. Zaitsev, V. Gusev, and B. Castagnede, "Luxemburg-Gorky Effect Retooled for Elastic Waves: A Mechanism and Experimental Evidence," Physical Review Letters **89**, 105502(1–4) (2002).

S7. V. Y. Zaitsev, V. E. Nazarov, and V. I. Talanov, "Experimental study of the self-action of seismoacoustic waves," Acoustical Physics **45**, 720–726 (1999).

S8. Staron L, Vilotte J-P and Radjai F, "Preavalanche instabilities in a granular pile", Phys. Rev. Lett. **89,** 204302 (2002).

S9. Staron L, Radjai F and Vilotte J-P, "Granular micro-structure and avalanche precursors", J. Stat. Mech. P07014 (2006).

Supplemental material – 2: Direct demonstration of the presence of numerous sub-micrometer asperities at the surface of the glass beads

Figure 1S shows an example of AFM image of the apparently optically smooth surface of a glass bead of 2 mm in diameter. Numerous asperities with 20-50 nm in height and radius 50-150 nm are visible. It can readily be estimated that, for a single macrosopic contact between the grains within the layer 20-50 nm in thickness near just touching each other surfaces, the total number of the mesoscopic asperities can easily reach $\sim 10^4$. Consequently, even if only 1% of those asperities (potential nano-contatcs) actually get in contact, i.e. become "closed" using the terminology of the present Letter, this already yields $\sim 10^2$ or even more nano-contacts per one visible intergrain macro-contact with just touching surfaces.

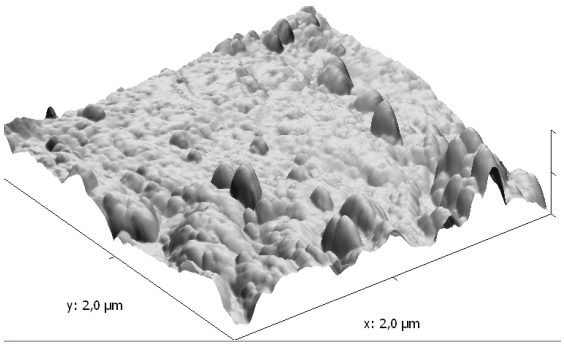

Fig. 1SS. AFM image of sub-micrometer asperities with heights 20-50 nm and radii 50-150 nm present at the surface of a glass bead

Furthermore, it can be noted that comparable amounts of weak adhesion-supported mesoscopic contacts can appear not only at the surfaces of such loose macro-contacts, but also within the annulus zone around each stronger-loaded "skeleton" macro-contact, i.e., within the region where the macro-contact surfaces are separated by the distance equal to typical heights of the sub-micrometer asperities about ~20-50 nm shown in Fig. 1SS.

For such a proportion between the visible intergrain contacts and tiny nano-scale asperities, the contribution of the latter can significantly dominate in the amplitude of the nonlinearly generated second harmonic or demodulated signal. Indeed, let us recall that the nonlinear component (e.g., the second harmonic for simplicity) of the elastic force developed at a Hertzian contact for a given displacement amplitude is proportional to the square root of the contact radius (see, for example, refs.[13,14,16] in the Letter). Since for a macroscopic intergrain contact with radius $R = 1$ mm and for a nano-scale asperity with radius $r = 100$ nm sitting on the surface, displacements are equal, the ratio between the second-harmonic amplitudes of the elastic force for those contacts scales as $F_R^{2\omega} / F_r^{2\omega} = (R/r)^{1/2} = 10^2$. Therefore, for the above estimated amount of $\sim 10^2$ tiny nano-scale contacts per one visible contact, the contributions of the macroscopic and nano-scale contacts to the nonlinearity-produced force component should already be comparable even under the assumption of equal initial pre-strain of all contacts. Furthermore, in contrast to the discussed in the Letter weak nano-scale contacts closed by inter-molecular interaction forces, the macroscopic contacts forming the material skeleton are actually precompressed by a value significantly (typically 1-2 orders) exceeding the acoustic displacement amplitude. Therefore, since the contact nonlinearity is inversely proportional to its prestrain [13,18,19], the strong macroscopic contacts forming the material skeleton oscillate in a much less nonlinear regime than the weak contacts formed by nano-scale asperities. Consequently, the nonlinear contribution of the apparently tiny, but numerous and strongly nonlinear nano-scale contacts can significantly exceed the nonlinearity of visible intergrain contacts composing the granular material skeleton that mostly determines the linear elastic moduli.

This explains why in apparently motionless granular packing the nonlinear-acoustic signal level can spontaneously vary in time up to several times (and even an order of magnitude) due to gradual closing of the nano-scale contacts under the action of thermal fluctuations and other weak mechanical perturbations. Depending on the sign and details of temporal shape such weak perturbations eventually can either break closed nano-contacts or in contrast promote their closing through the mechanisms of jumps between those closed and open states as discussed in the Letter text.